OAK RIDGE
NATIONAL LABORATORY
MANAGED BY UT-BATTELLE
FOR THE DEPARTMENT OF ENERGY

ORNL/TM-2011/259

Low Velocity Sphere Impact of a Soda Lime Silicate Glass

A. A. Wereszczak,* E. E. Fox,
T. G. Morrissey, and D. J. Vuono
Ceramic Science and Technology Group
Materials Science and Technology Division
Oak Ridge National Laboratory
Oak Ridge, TN 37831-6068

* Principal Investigator
wereszczakaa@ornl.gov

Publication Date: October 2011

Prepared by the
OAK RIDGE NATIONAL LABORATORY
Oak Ridge, Tennessee 37831
managed by
UT-BATTELLE, LLC
for the
U.S. DEPARTMENT OF ENERGY
Under contract DE-AC05-00OR22725

US ARMY TARDEC
DISTRIBUTION STATEMENT A.
Approved for public release; distribution unlimited.

UT-BATTELLE
ORNL-27 (4-00)

DOCUMENT AVAILABILITY

Reports produced after January 1, 1996, are generally available free via the U.S. Department of Energy (DOE) Information Bridge:

Web site: http://www.osti.gov/bridge

Reports produced before January 1, 1996, may be purchased by members of the public from the following source:

National Technical Information Service
5285 Port Royal Road
Springfield, VA 22161
Telephone: 703-605-6000 (1-800-553-6847)
TDD: 703-487-4639
Fax: 703-605-6900
E-mail: info@ntis.fedworld.gov
Web site: http://www.ntis.gov/support/ordernowabout.htm

Reports are available to DOE employees, DOE contractors, Energy Technology Data Exchange (ETDE) representatives, and International Nuclear Information System (INIS) representatives from the following source:

Office of Scientific and Technical Information
P.O. Box 62
Oak Ridge, TN 37831
Telephone: 865-576-8401
Fax: 865-576-5728
E-mail: reports@osti.gov
Web site: http://www.osti.gov/contact.html

This report was prepared as an account of work sponsored by an agency of the United States Government. Neither the United States government nor any agency thereof, nor any of their employees, makes any warranty, express or implied, or assumes any legal liability or responsibility for the accuracy, completeness, or usefulness of any information, apparatus, product, or process disclosed, or represents that its use would not infringe privately owned rights. Reference herein to any specific commercial product, process, or service by trade name, trademark, manufacturer, or otherwise, does not necessarily constitute or imply its endorsement, recommendation, or favoring by the United States Government or any agency thereof. The views and opinions of authors expressed herein do not necessarily state or reflect those of the United States Government or any agency thereof.

TABLE OF CONTENTS

LIST OF FIGURES

Figure **Page**

LIST OF FIGURES (Continued)

Figure **Page**

LIST OF TABLES

EXECUTIVE SUMMARY

This report summarizes TARDEC-sponsored work at Oak Ridge National Laboratory (ORNL) during the FY11 involving low velocity (< 30 m/s or < 65 mph) ball impact testing of Starphire soda lime silicate glass. The intent was to better understand low velocity impact response in the Starphire for sphere densities that bracketed that of rock. Five sphere materials were used: borosilicate glass, soda-lime silicate glass, steel, silicon nitride, and alumina. A gas gun was fabricated to produce controlled velocity delivery of the spheres against Starphire tile targets. Minimum impact velocities to initiate fracture in the Starphire were measured and interpreted in context to the kinetic energy of impact and the elastic property mismatch between the any of the five sphere-Starphire-target combinations.

The primary observations from this low velocity (< 30 m/s or < 65 mph) testing were:

- Frictional effects contribute to fracture initiation.
- Spheres with a lower elastic modulus require less force to initiate fracture in the Starphire than spheres with a higher elastic modulus.
- Contact-induced fracture did not initiate in the Starphire SLS for impact kinetic energies < 150 mJ. Fracture sometimes initiated or kinetic energies between ~ 150 - 1100 mJ; however, it tended to occur when lower elastic modulus spheres were impacting it. Contact-induced fracture would always occur for impact energies > 1100 mJ.
- The force necessary to initiate contact-induced fracture is higher under dynamic or impact conditions than it is under quasi-static indentation conditions.
- Among the five used sphere materials, silicon nitride was the closest match to "rock" in terms of both density and (probably) elastic modulus.

1. INTRODUCTION

The impact of rock onto glass or transparent windshields is somewhat of a common issue with vehicles. A rock can come in contact with the windshield by multiple means including being kicked up by another passing vehicle. Impact velocities will be in the range of the speed that the vehicles are moving at. When a rock impacts the glass windshield, one of two things will occur; either the glass will elastically respond and no damage is initiated or it will be permanently damaged (e.g., chipping or cracking). Such permanent damage can cause overall weakening of the window, or affect the optical properties of the glass, or both. By studying and quantifying the effect of rock impact on glass the potential is established to improve resistance to the onset of undesirable permanent damage.

The meaning of the word “rock” can be quite ambiguous from a technical perspective. Rocks obviously can have different geometries (e.g., sizes and shapes) and compositions (e.g., densities and other material properties such as elastic modulus). Rocks generally have unsymmetrical shapes with many edges. When a rock strikes a glass, one of many possible complicated and unpredictable loading scenarios can result based on its geometry. It therefore can be difficult to assess a window's (i.e., target's) impact resistance when the impactor (i.e., rock or stone) can have so many independent parameters.

A sphere can be used to lessen the complexity of the event of a rock striking a glass target. A sphere of given size or diameter, density, and other physical properties can mimic or bracket those of a rock. The area and impact response of the target will be the same no matter what part of the sphere impacts it. This removes the unpredictable randomness of multiple edges and rotations of rock impact from the experiment. As we will show, it produces greater depth of understanding of the target and target material response. Additionally, sphere impact testing enables the use of established and simple Hertzian analytical modeling and subsequent interpretations. Ultimately though, an improved resistance to damage initiation with a spherical impact translates to an increased resistance to damage from an actual rock strike.

In the present study, the sphere impact response of a transparent armor grade soda-lime-silicate (SLS) was examined at velocities up to ~ 30 m/s (~ 65 mph). Five different ball materials were used for the impact testing and were chosen because their range of densities bracket realistic rock densities. It was anticipated that the amount of kinetic energy of impact (related to sphere material density and impact velocity) would dictate the response of the SLS targets.

Another feature of the sphere impact found to affect target material response at these low velocities was elastic property mismatch between sphere and target materials. However, that is not necessarily a surprise upon further thought. It is known the elastic property mismatch between a spherical indenter and target material will affect the force at which Hertzian ring cracking initiates in the target because of friction [1]. At higher velocities (i.e., higher kinetic energies), this contributing "elastic property mismatch effect" remains finite but becomes insignificant compared to the increasing magnitude and dominance of kinetic energy. But at these low velocities (< 30 m/s or < 65 mph), it was found that reducing the elastic modulus (i.e., lower stiffness) of the sphere material resulted in greater ease (i.e., lower impact forces) of initiating permanent damage in the target SLS glass.

2. BASICS OF SPHERICAL IMPACT

2.1. Estimating Impact Force from Impact Velocity

When a sphere impacts a target the amount of stress is determined by the impulse and the amount of contact area the force is acting on [2]. For spherical or Hertzian contact loading, and assuming frictionless contact (as classical Hertzian analysis inherently does), the stress, $\sigma_{rad\text{-}max}$, required to initiate ring cracking can be determined using

$$\sigma_{rad-\max} = \frac{1-2\nu}{2\pi}\frac{RCIF}{a^2} \quad , \tag{1}$$

where *RCIF* is the ring crack initiation force, v is Poisson's ratio of the target material, and a is the contact radius at the applied *RCIF*. The contact radius is determined using

$$a = \left(\frac{3}{4} k \bullet RCIF \bullet R \right)^{1/3} \quad , \tag{2}$$

where R is the sphere radius, and

$$k = \frac{1 - \nu_s^2}{E_s} + \frac{1 - \nu_t^2}{E_t} \quad , \tag{3}$$

where E is the Young's modulus, and subscripts s and t represent the sphere and target, respectively.

At rock strike velocities, the velocity of impact is (or may be) known but not the associated applied force. Knight *et al.* [3] developed a relationship to calculate force from impact velocity by equating the kinetic energy of the sphere before impact to that of the total work, or

$$\frac{1}{2} \left(\frac{4}{3} \pi \rho R^3 \right) V^2 = \int_0^{Z_{Max}} P(z) dz \quad , \tag{4}$$

where ρ is the density of the sphere, V is the velocity of the sphere, and z is calculated by

$$z = \frac{a^2}{R} \quad . \tag{5}$$

This allows for the estimation of the maximum force, P_{max}, from a dynamic impact as described by Timoshenko and Goodier [4] or

$$P_{Max} = \left(\frac{5}{3}\pi\rho\right)^{3/5}\left(\frac{3}{4}k\right)^{-2/5} V^{6/5}R^2 \quad . \tag{6}$$

If the impact initiates a ring crack, then P_{Max} in Eq. 6 can be equated to the ring crack initiation force (*RCIF*), or

$$RCIF = P_{Max} = \left(\frac{5}{3}\pi\rho\right)^{3/5}\left(\frac{3}{4}k\right)^{-2/5} V^{6/5}R^2 \quad . \tag{7}$$

The calculated impact *RCIF* using Eq. 7 can then be compared to the *RCIF* measured by quasi-static spherical indentation testing. Note that RCIF in Eq. 7 is independently related to sphere density (ρ) and the elastic properties of the of sphere and target (i.e., k).

It should be noted that the above equations are valid provided all deformation is linear elastic. If plastic or permanent deformation were to occur prior to ring crack initiation in either the sphere or target, then this introduces a violation of those assumptions and a level of complexity in the stress analysis that is beyond the scope of this report. Knight *et al.* [3] saw this Hertzian theory assumption break down with steel spheres impacting SLS glass, and as will be presented later in this report, the effects of the violation of that assumption was observed in the present study too for steel spheres.

2.2. Comparing Different Ball Materials

Under contact conditions, spheres of different material will elastically deform differently when pushed against the same target material with the same applied force. That is because those sphere materials have different elastic properties and therefore will exhibit different Poisson's effect responses. While the same sphere diameter (12.7 mm) was used in all tests in the present study, ideally, to perform contact response studies involving different sphere materials, diameters should be used in context to the ball material elastic properties so that the same contact area (and contact stress) are produced for the same applied compressive force for each sphere material. This is important because it enables a confident comparison between ring crack initiations

generated by balls made from dissimilar materials, namely, the target material should ring crack at the same applied compressive force with [sphere] materials of these two radii if there is a sustained frictionless Hertzian contact and if both the indenter and target material remain linearly elastic up to this force [1].

The necessary sphere sizes for dissimilar materials can be calculated by using the analysis of Johnson, *et al.* [5], namely

$$R_1\left[\frac{1-\nu_1}{G_1}+\frac{1-\nu_t}{G_t}\right]=R_2\left[\frac{1-\nu_2}{G_2}+\frac{1-\nu_t}{G_t}\right] \tag{7}$$

or

$$\frac{R_2}{R_1}=\frac{\frac{1-\nu_1}{G_1}+\frac{1-\nu_t}{G_t}}{\frac{1-\nu_2}{G_2}+\frac{1-\nu_t}{G_t}} \tag{8}$$

where R is sphere radius, v is Poisson's ratio, and G is shear modulus with subscripts *1*, *2* and *t* representing sphere materials *1* and *2*, and the target material, respectively. The target material in this study was Starphire SLS glass and material *1* was chosen to be the SLS sphere material because of its almost identical properties to the target material. With these designations, the calculated value of R_2 will result in the necessary sphere size for a given material (and its elastic properties) to produce the same contact radius as the SLS sphere at a given force.

Even though the same sphere diameter was used in all these, their produced impact conditions can still be correlated by developing a ratio of force, contact area, and stress using Eq. 1. With the known ring crack initiation stress, the force needed to produce the same stress with the constant contact radius, Eq. 2, (calculated using the sphere radius from Eq. 8) the normalized stress can be determined according to,

$$\frac{1-2\nu}{2\pi}\frac{RCIF_{ACT}}{a_{ACT}^2}=\frac{1-2\nu}{2\pi}\frac{RCIF_{NORM}}{a_{NORM}^2} \tag{9}$$

which can be simplified to

$$\frac{P_{ACT}}{a_{ACT}^2}=\frac{P_{NORM}}{a_{NORM}^2}\quad . \tag{10}$$

Equation 10 allows for a normalized RCIF, P_{NORM}, to be calculated and compared.

To represent this mismatch of elastic properties between the target and sphere, the Dundurs parameter, β, is a useful concept to utilize. β is useful because it describes both the magnitude and direction of the elastic modulus mismatch between the contact pair. A positive β defined here means the sphere's elastic properties produce greater stiffness than that of the target material while a negative β means the target is stiffer than the sphere. The sign of β also describes if the sphere or target is restricting the movement of the other under shear traction loading. β can be calculated from [6]

$$\beta=\frac{\frac{1-2\nu_t}{G_t}-\frac{1-2\nu_s}{G_s}}{2\left(\frac{1-\nu_t}{G_t}-\frac{1-\nu_s}{G_s}\right)} \tag{11}$$

where ν is Poisson's ratio, and G is shear modulus with subscripts s and t representing the sphere and target, respectively.

Using the normalized diameters and forces from Eq. 10, the RCIF as a function of elastic properties and Dundurs Parameter was examined in this study. As will be shown, elastic property mismatch between the sphere and target material was found to affect RCIF response in the target SLS glass. That dependence in turn illustrates that frictional traction between the sphere and target glass is affecting Hertzian fracture initiation.

2.3. Ring Crack Initiation at Dynamic vs. Quasi-Static Conditions

The effects of the mismatch of elastic properties between the sphere and target on ring crack initiation (i.e., fracture initiation) have not been systematically considered in (dynamic) ball impact even though they are well established in spherical indentation (quasi-static) testing. Quasi-static indention testing, when teamed with acoustic emission detection, can easily identify the RCIF. RCIF is not so easy to detect during real-time ball impact testing, but velocity is. By using Eq. 7, the RCIF of ball impact testing can be estimated for different ball materials by identifying the velocity at which ring crack initiations (a dynamic RCIF) and compared to RCIF responses measured quasistatically with spherical indentation. A difference in RCIF response will be indicative of rate-effects affecting the dynamic RCIF.

As will be shown, a rate-dependence on sphere impact RCIF was observed. Additionally, it appeared that friction was still contributing to the RCIF.

3. GAS GUN, TARGET GLASS, SPHERE IMPACTERS, AND SABOT

3.1. Gas Gun Description

A gas gun system was constructed from guidance provided from Purdue University. The air supply and barrel of the gas gun is shown in Fig. 1. The system uses compressed air controlled to predetermined pressure, which is then rapidly released via a regulator into a barrel. The barrel is preloaded with a sphere held by a sabot and the released air propels them both towards the glass sample. At the end of the muzzle the sabot is stopped propelling the sphere toward the glass target.

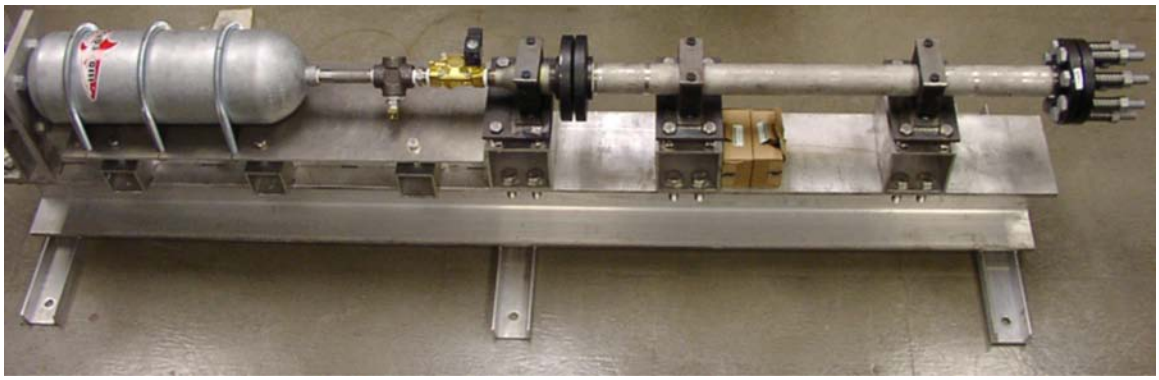

Figure 1. Gas gun assembly for low velocity ball impact testing.

The sphere passes through a parallel beam laser detection system. The velocity measurement system and impact area can be seen in Fig. 2. The laser beams are 100-mm-spaced and the sphere's time-of-flight is measured. They are visible by the red dots shown in Fig. 3. The parallel laser beams were oriented vertically so the projectile path of the sphere would interfere with the laser regardless its arch. The muzzle end, glass target, and general impact area are enclosed in plastic to maintain safe operating conditions.

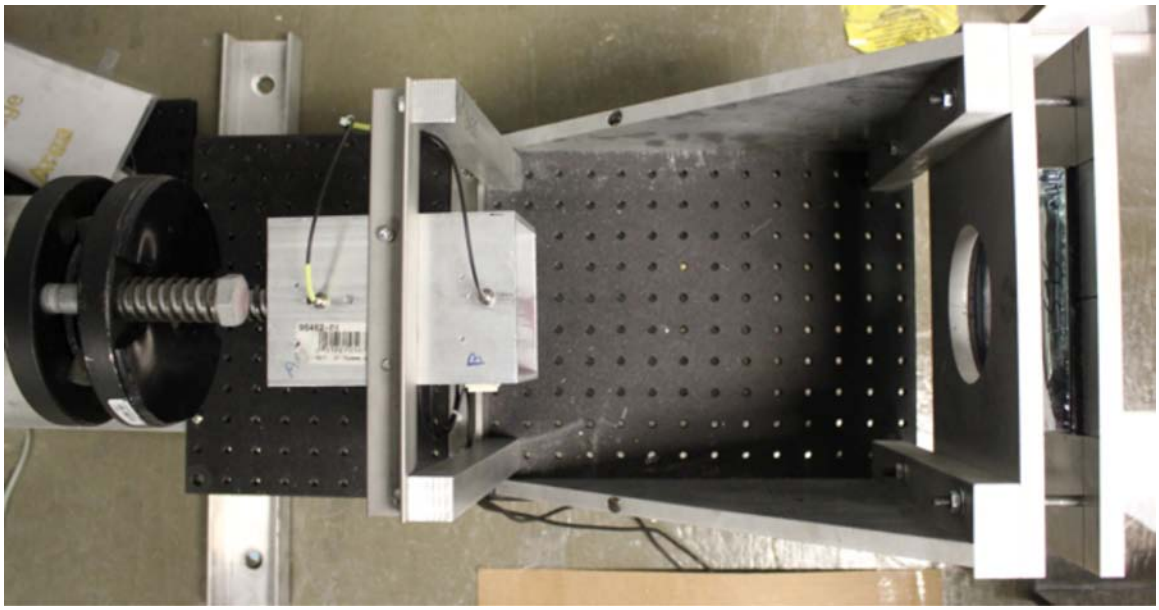

Figure 2. Top view showing end of barrel (left), velocity measurement device, and target glass (right of circular cut-out).

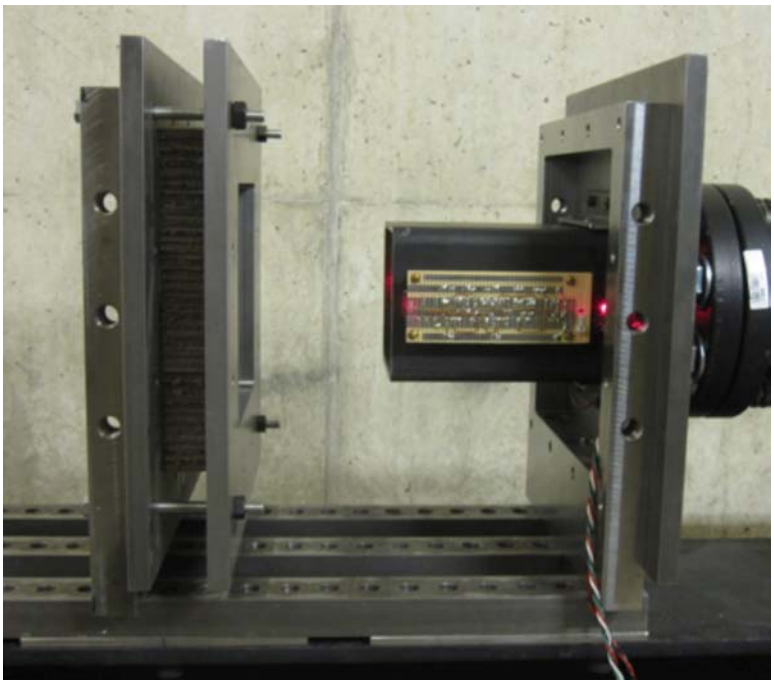

Figure 3. Velocity measurement laser system.

The velocity data was recorded using an in-house developed LabView software program and a high-speed data acquisition card (National Instruments, Austin, TX). The time-of-flight data were collected with the parameters listed in Table .

Table I. Data collection parameters for velocity recording software.

Minimum Sample Rate (Hz)	4.0×10^4
Minimum Number of data points	2000
Resolution (sec)	2.5×10^5
Total Time (sec)	0.05

3.2. Target Glass Description

The target glass tiles were a commercially available soda-lime-silicate glass (Starphire, PPG, Pittsburgh, PA) and had dimensions of 10.2 x 10.2 x 1.9 cm. This glass is a tin float glass, and the tin side was tested with all tiles. Its density was measured to be 2.49 g/cm^3. The elastic modulus and Poisson's ratio were measured with resonance ultrasound spectroscopy and were 73.1 GPa and 0.203, respectively. A target glass in position can be seen in the right of Fig. 2. Detailed descriptions of many of this glass's properties and characteristics have been reported by the authors [7].

3.3. Sphere Description

Sphere materials were chosen with rock density in mind. Rock density can obviously vary from region to region. As an example, the average density was measured with several rocks picked up off the ground on the ORNL campus and was 2.80 g/cm^3. Spheres with material of that density were not commercially available, so that density was bracketed using five different sphere materials. They, in order of increasing density as listed in Table II, were a borosilicate (BS) glass, a soda lime silicate (SLS) glass, silicon nitride (Si_3N_4), aluminum oxide or alumina (Al_2O_3), and 52100 (low chrome) steel. Images of each are shown in Fig. 4. A one-half-inch (12.7 mm) diameter was used in all testing. The balls were purchased from commercial suppliers (Salem Ball, Canton, CT, for the BS and SLS glasses, McMaster-Carr, Atlanta, GA, for the alumina and steel, and Cerbec, East Granby, CT, for the silicon nitride balls).

Table II. Diameter and densities of materials for sphere impact testing.

Material	Diameter (cm)	Mass (g)	Density (g/cm^3)
Borosilicate	1.270	2.3796	2.221
Soda Lime Silicate	1.270	2.6957	2.516
Si_3N_4	1.270	3.3910	3.165
Alumina	1.270	4.1804	3.901
Steel	1.270	8.3597	7.802

Figure 4. Spheres used for impact testing (from left to right): borosilicate (BS) glass, alumina (Al_2O_3), soda-lime silicate (SLS) glass, steel, and silicon nitride (Si_3N_4).

The elastic modulus and Poisson's ratio of the spheres were determined using resonant ultrasounds spectroscopy (RUS) using a method developed by the author [8]. Their values are shown in Table III along with their calculated Dundurs parameter with respect to Starphire SLS glass (Eq. 11), and normalization diameter relative to 12.7 mm diameter SLS glass sphere (Eq. 8).

Table III. Elastic properties, constant contact area diameter, and actual ball diameters.

Sphere Material	Elastic Modulus - E - (GPa)	Poisson's Ratio - ν –	Shear Modulus - G - (GPa)	Eq. 8 Ball Dia. - $2R$ - (mm)	Used Ball Dia. - $2R$ - (mm)	Dundurs Parameter* - β - (unitless)
Borosilicate glass	61.9	0.199	25.8	11.46	12.70	-0.033
Soda Lime Silicate glass	73.8	0.245	29.6	12.70	12.70	0.023
Steel	204	0.282	79.6	18.62	12.70	0.200
Si_3N_4	300	0.207	124	20.13	12.70	0.227
Al_2O_3	371	0.220	152	20.93	12.70	0.253

* Calculated using Eq. 11 for the given sphere material against Starphire SLS glass target.

3.4. Sabot Description

A sabot was used for the sphere shooting. The sabots were cast from a rigid polyurethane foam (FOAM-iT!® 15, Smooth-On, Inc., Easton, PA) and were formed in a shape to retain a 12.7 mm diameter sphere. The sabot cradles the sphere as it accelerates down the barrel. At the muzzle end of the barrel the fast traveling sabot was abruptly stopped launching the sphere toward the glass sample.

4. EXPERIMENTAL PROCEDURE

4.1. Calibration and Unit Conversions

The ratio of gas gun pressure to produced sphere velocity was determined in order to control the approximate velocity the sphere would hit the target. The relationship is shown in Fig. 5.

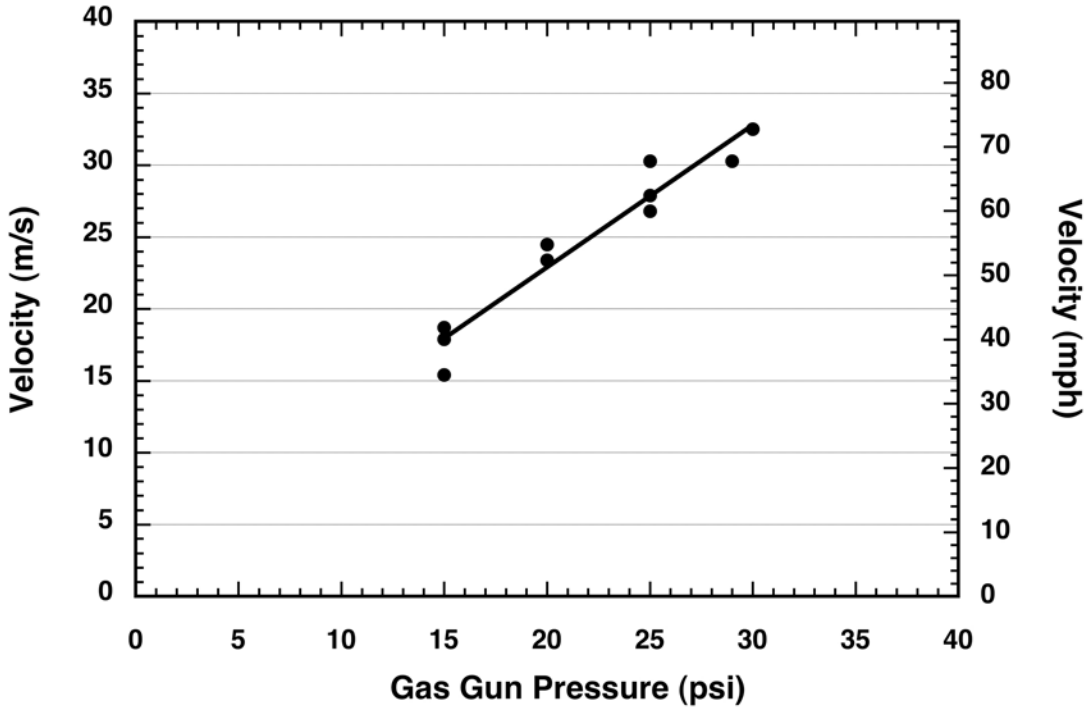

Figure 5. Gas gun pressure and resulting velocity.

The mass of the sabot was much greater than the mass of the sphere for all five materials therefore it was assumed that all spheres launched at approximately the same velocity for a given pressure. Regardless, the velocity of each launch was recorded. Occasionally the velocity measurement system failed to record. In those instances, the velocity was estimated using the trend shown in Fig. 5. Metric and English units of velocity were both used, and their unit conversions are illustrated in Fig. 6 and listed in Eqs. 12-14.

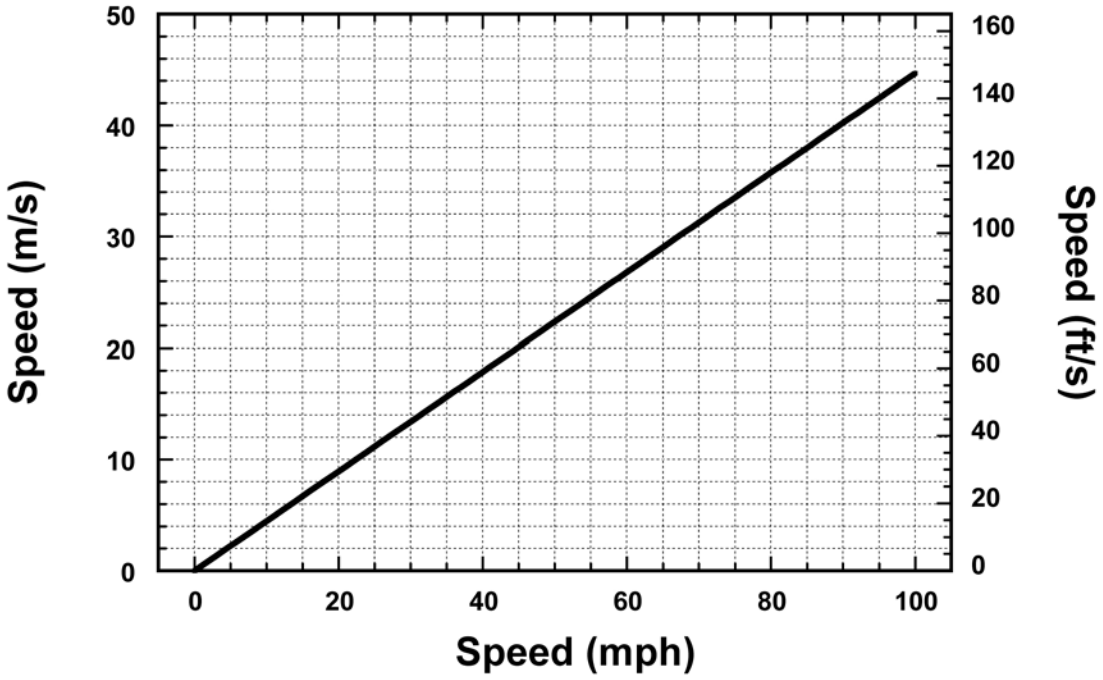

Figure 6. Velocity conversions between m/s, mph, and ft/s.

$$1.00\ m/s = 3.28\ ft/s = 2.24\ \text{mph} \tag{12}$$

$$1.00\ \text{mph} = 1.47\ ft/s = 0.447\ m/s \tag{13}$$

$$1.00\ ft/s = 0.682\ \text{mph} = 0.305\ m/s \tag{14}$$

4.2. Impact Test Procedure

The Starphire SLS glass tile was loaded into position in the tile holder and oriented to be struck on its tin side. The Starphire SLS glass tile was sandwiched between two medium density rubber gaskets each having 100-mm-diameter holes co-located with the 100-mm-diameter hole in the holders (seen at far right in Fig. 2). There is a bottom rubber gasket to keep the placement height constant and position the target glass to be struck in the approximate center of the glass tile (100-mm-diameter exposed). The four bolts that compressed the rubber gaskets were torqued to 5 ft•lb (7 N•m). The relatively thick glass, coupled with the firm gripping of their margin for the sphere impact testing, likely results in very minimal deflection of the tiles occurring during the impact event. In support of that, no tiles ever fractured from bending.

The sabot and sphere were loaded on the breach side of the barrel and the barrel connected to the air gas supply. The gas chamber was adjusted to the desired pressure using input and blow-off valve switches. With the safety shields positioned, the main valve of the gas chamber was switched open to release the compressed air into the barrel behind the sabot, thusly launching it. The velocity of the ejected sphere was recorded and the damage to the target sample optically examined with a compound optical microscope. A new sphere was always used for each test.

Impact damage to the tile was classified into five groups; no damage, scuff, ring crack with small cone crack, ring crack with medium cone crack, and ring crack with large cone cracks. The scuff designation indicated that a frictional or sliding event had occurred without ring and cone cracking. The small, medium and large cone cracks were designated to the cone crack propagating to a depth of approximately one-third, two-thirds, or all the way through the glass target thickness. The crack initiation force was defined as the lowest velocity at which any size cone crack was seen (i.e., velocity necessary to initiate fracture).

4.3. Quasi-Static Indentation

Quasi-static spherical indentation was performed using an electromechanical test frame. The impact RCIF was shown in Eq. 7 to be independently related to sphere density and elastic properties of the sphere and target; however, for quasi-static indentation, sphere density does not affect RCIF, so this is a potential means to deconvolute their effects on RCIF. A schematic of the experimental setup is shown in Fig. 7. The same 12.7-mm-diameter spheres (Fig. 4) used for the impact testing were used as spherical indenters. The glass tiles used for indentation were the same target Starphire SLS glass tiles used for impact testing. The indentation was performed on the tin side of the glass just like the tin side was impact tested. A displacement rate of 0.0001 mm/s was used to compressively load the glass tile until crack initiation occurred followed by rapid unloading. Acoustic emission was monitored to determine the moment of ring crack initiation and its associated compressive force. Each indentation test occurred in an undamaged portion of the Starphire SLS glass tile. At least 16 indentation tests were performed with all five ball materials, and their average, standard deviation, minimum, and maximum values were determined.

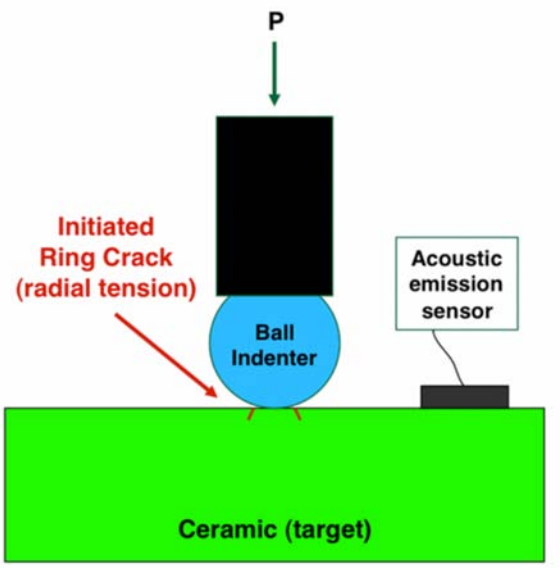

Figure 7. Schematic drawing of the ring crack initiation test configuration. An acoustic emission sensor was used to detect an acoustic event that was then linked to the ring crack initiation force. Target material is Starphire SLS glass.

5. RESULTS AND DISCUSSION

5.1. Impact Response

The identified minimum velocities needed to initiate ring crack initiation (i.e., fracture) in the Starphire SLS glass tiles for each of the five sphere materials are shown in Table IV. The complete list of tests and results are shown in Appendix I. The estimated ring crack initiation force (RCIF) values listed in Table IV were calculated using Eq. 7 with those listed velocities. The maximum radial tensile stress was calculated using Eq. 1. The kinetic energy was calculated using the classical formulation of $1/2 \bullet m \bullet V^2$ where m is mass of the sphere.

Table IV. Estimated ring crack initiation force from impact testing responses.

Sphere Material	Velocity (m/s)	RCIF (N)	Maximum Radial Tensile Stress (MPa)	Kinetic Energy (mJ)
Borosilicate glass	12	3778	576	171
SLS glass	12	4540	641	194
Steel	17	20459	1256	1208
Si_3N_4	12	8518	971	244
Al_2O_3	9.8	7897	963	201

5.2 Indention Response

The summary statistics from the quasi-static spherical indention testing are shown in Tables V-VI for the 12.7 mm diameter balls and for the normalized ball diameters. Only ring crack initiation force is collected from this test. Examples of ring cracks produced by the five spheres are shown in Fig. 8. Those ring cracks in Fig. 8 were generated with the minimum RICFs in each set RCIF distribution pertaining to what is shown in Table V.

Table V. Ring crack initiation force (RCIF) from quasi-static spherical indentation testing using 12.7 mm diameter spheres.

Sphere Material	Average RCIF (N)	Std Dev RCIF (N)	Min RCIF (N)	Max RCIF (N)
Borosilicate glass	1954	1082	440	3509
SLS glass	632	350	375	1650
Steel	3471	1482	1613	6554
Si_3N_4	2820	1137	1295	5884
Al_2O_3	3064	1346	1255	7069

Table VI. Ring crack initiation force (RCIF) from quasi-static spherical indentation testing after diameter normalization according to Eq. 10.

Sphere Material	Eq. 8 Diameter (mm)	Average RCIF (N)	Std Dev RCIF (N)	Min RCIF (N)	Max RCIF (N)
Borosilicate glass	11.46	1826	1011	411	3279
SLS glass	12.70	591	327	351	1541
Steel	18.62	3243	1385	1507	6123
Si_3N_4	20.13	2634	1063	1210	5497
Al_2O_3	20.93	2862	1257	1173	6604

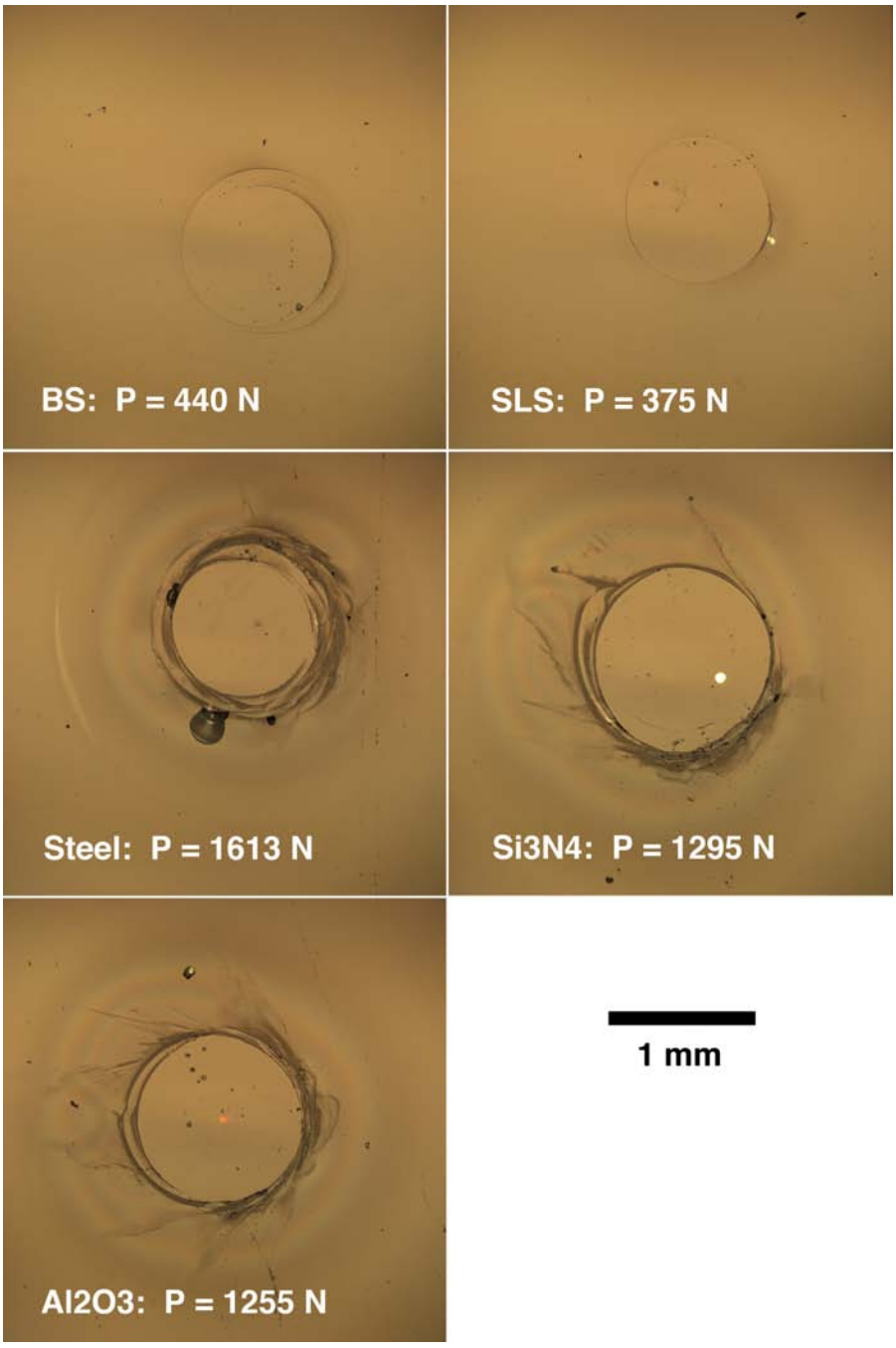

Figure 8. Comparison of low valued RCIFs for each of the five sphere materials.

5.3 Ring Crack Initiation Force - Quasi-Static vs. Impact

Spheres of a lower elastic modulus required less force to initiate a ring crack in the target materials, and that was true for both quasi-static spherical indentation testing and impact testing. This is illustrated in Fig. 9 when RCIF is plotted against the ball material elastic modulus and in Fig. 10 when plotted against Dundurs Parameter. The RCIF response with the steel spheres, unlike those with the other four materials, are not well-fitted by a linear line. This is due to the likelihood that the steel ball is deforming, owing to its relatively low yield stress, resulting in an increase in the radius of curvature and a lower applied radial tensile stress being produced in the target material. The other four materials remain linear elastic. This outlier behavior with steel has been observed before by the author with spherical indentation [1, 8].

The force necessary to initiate ring cracking is higher under dynamic conditions than it is under quasi-static conditions. Tillet [9] and Johnson *et al.* [5] reported similar differences in quasi-static and dynamic sphere tests that are shown in Figs. 10-11 but they did not offer a potential explanation other than indicating it was due to a "rate effect". The authors in the present study are not yet able to offer an explanation for the difference but hope to with additional work.

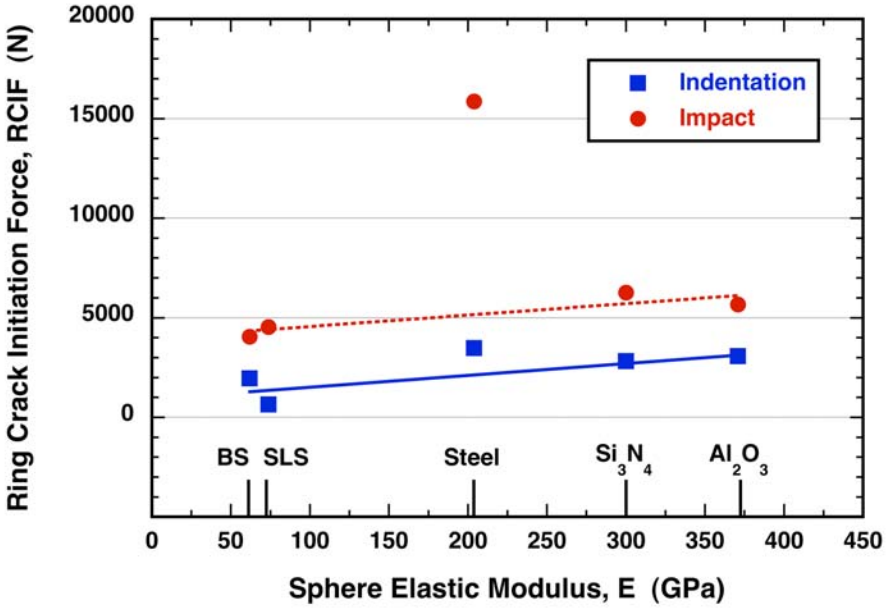

Figure 9. RCIF as a function of sphere material elastic modulus for 12.7 mm diameter spheres. Shown RCIF values from indentation are averages and those for impact testing are minimum values.

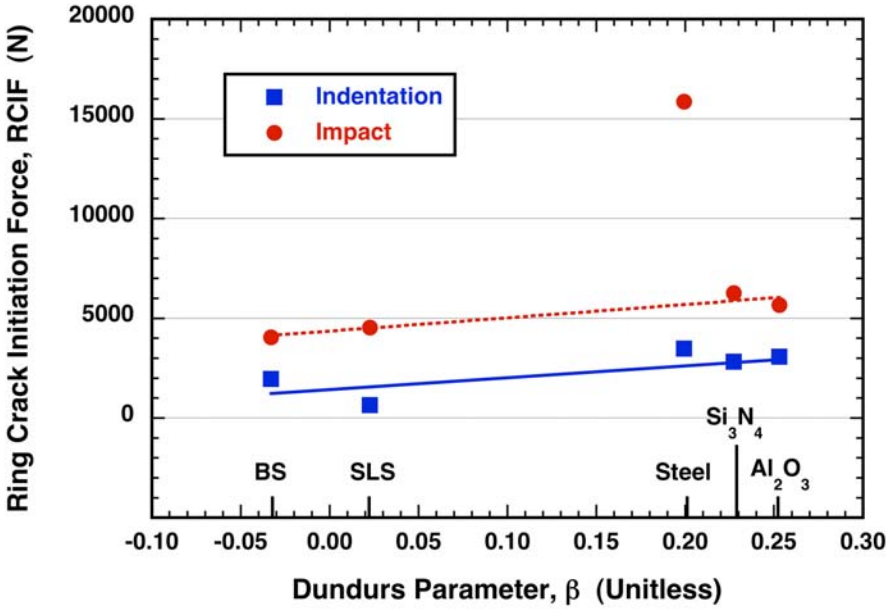

Figure 10. RCIF as a function of Dundurs Parameter for 12.7 mm diameter spheres. Shown RCIF values from indentation are averages and those for impact testing are minimum values.

In order to equivalently compare the quasi-static and dynamic RCIF responses, the sphere diameters and need to be normalized as listed in Table III. When those diameters are normalized, then Figs. 9-10 are transformed into what is illustrated in Figs. 11-12. The fact those fitted linear curves are *not* horizontal (i.e., RCIF independent of elastic properties) signifies that friction effects *are* contributing to the RCIF responses for both quasi-static and dynamic loadings.

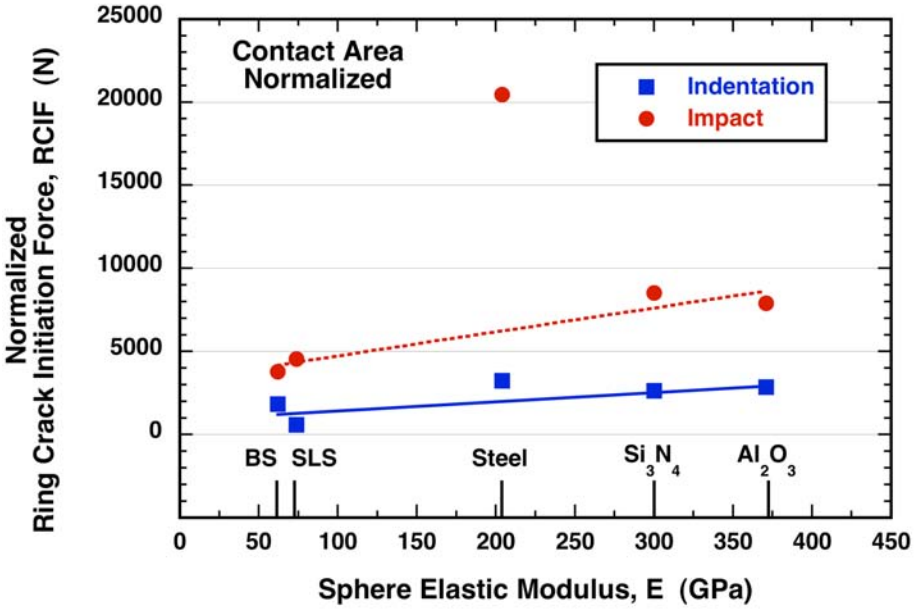

Figure 11. Normalized RCIF as a function of sphere material elastic modulus. The estimated RCIF values are based on the following material-ball-diameter combinations: BS:11.46mm, SLS:12.70mm, steel:18.62mm, Si_3N_4:20.13mm, and Al_2O_3:20.93mm.

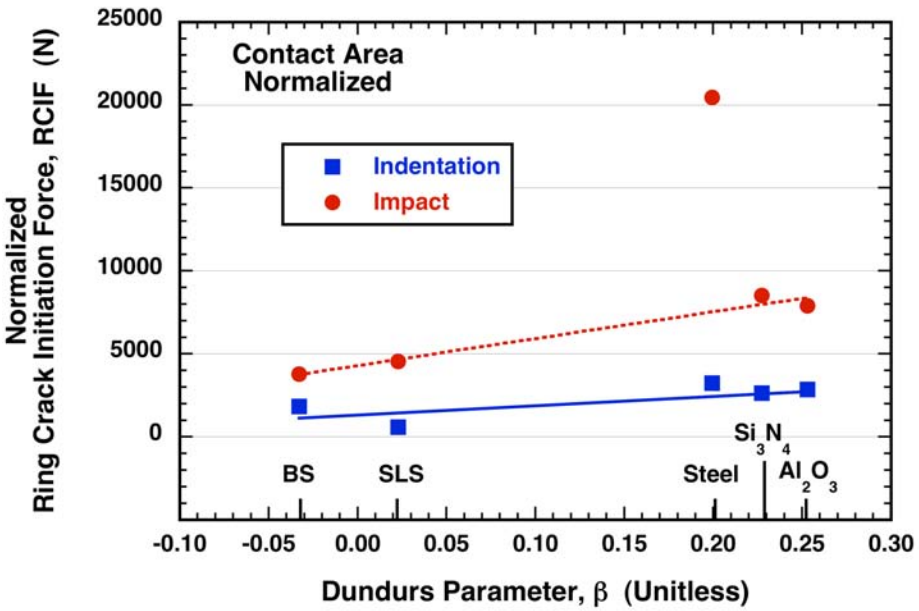

Figure 12. Normalized RCIF as a function of Dundurs Parameter. The estimated RCIF values are based on the following material-ball-diameter combinations: BS:11.46mm, SLS:12.70mm, steel:18.62mm, Si_3N_4:20.13mm, and Al_2O_3:20.93mm.

While the observed trends in Figs. 9-12 portray that elastic property mismatch between the sphere and the target glass is contributing to RCIF, the roll of kinetic energy must be considered too. The velocities and sphere materials listed in Appendix I were used to calculate kinetic energy ($1/2 \bullet m \bullet V^2$) and graphed as a function of each RCIF in Fig. 13. For kinetic energies less than about 150 mJ, no ring cracking initiated in the Starphire SLS. Between about 150 and 1100 mJ, ring cracking could initiation, but it tended to occur with lower elastic modulus spheres (i.e., elastic property mismatch, or low-valued β, along with friction contributed to RCIF). An illustration of that is shown in Fig. 14 for impacts at kinetic energies of approximately 500 mJ. For impact energies greater than 1100 mJ, ring crack initiation would always occur.

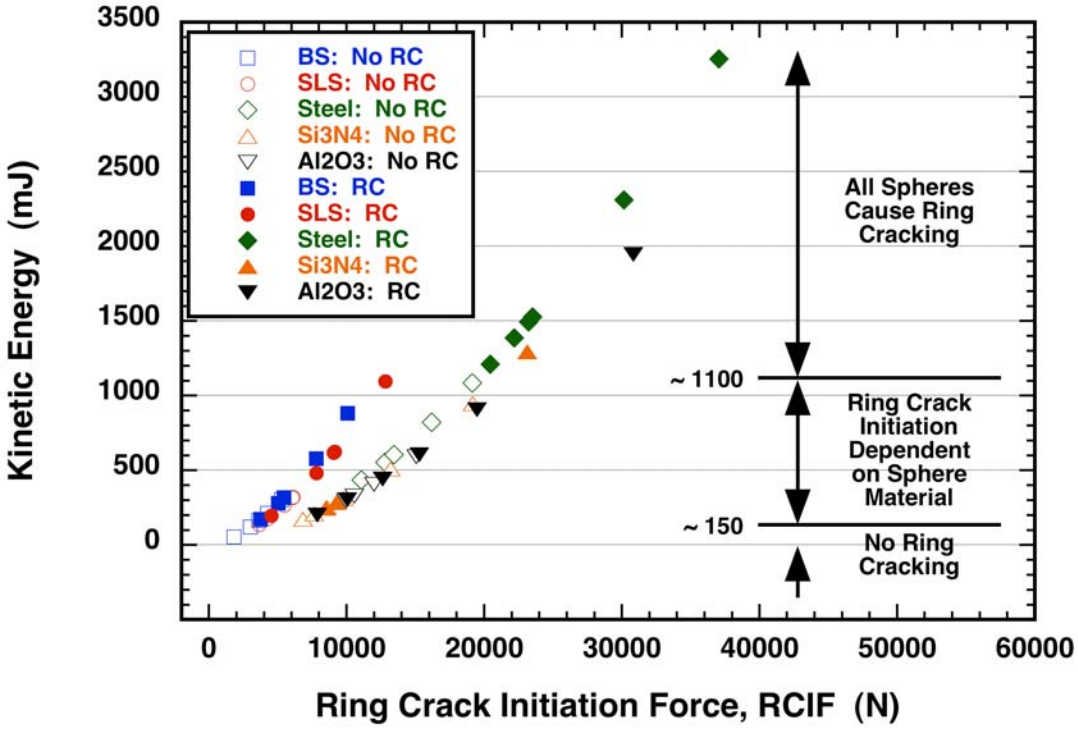

Figure 13. Relationship of kinetic energy and ring crack initiation force. Damage does not initiate in the target SLS glass for energies less than about 150 mJ, damage initiation is sphere material dependent between 150 and 1100 mJ, and the SLS ring cracks for all kinetic energies greater than 1100 mJ.

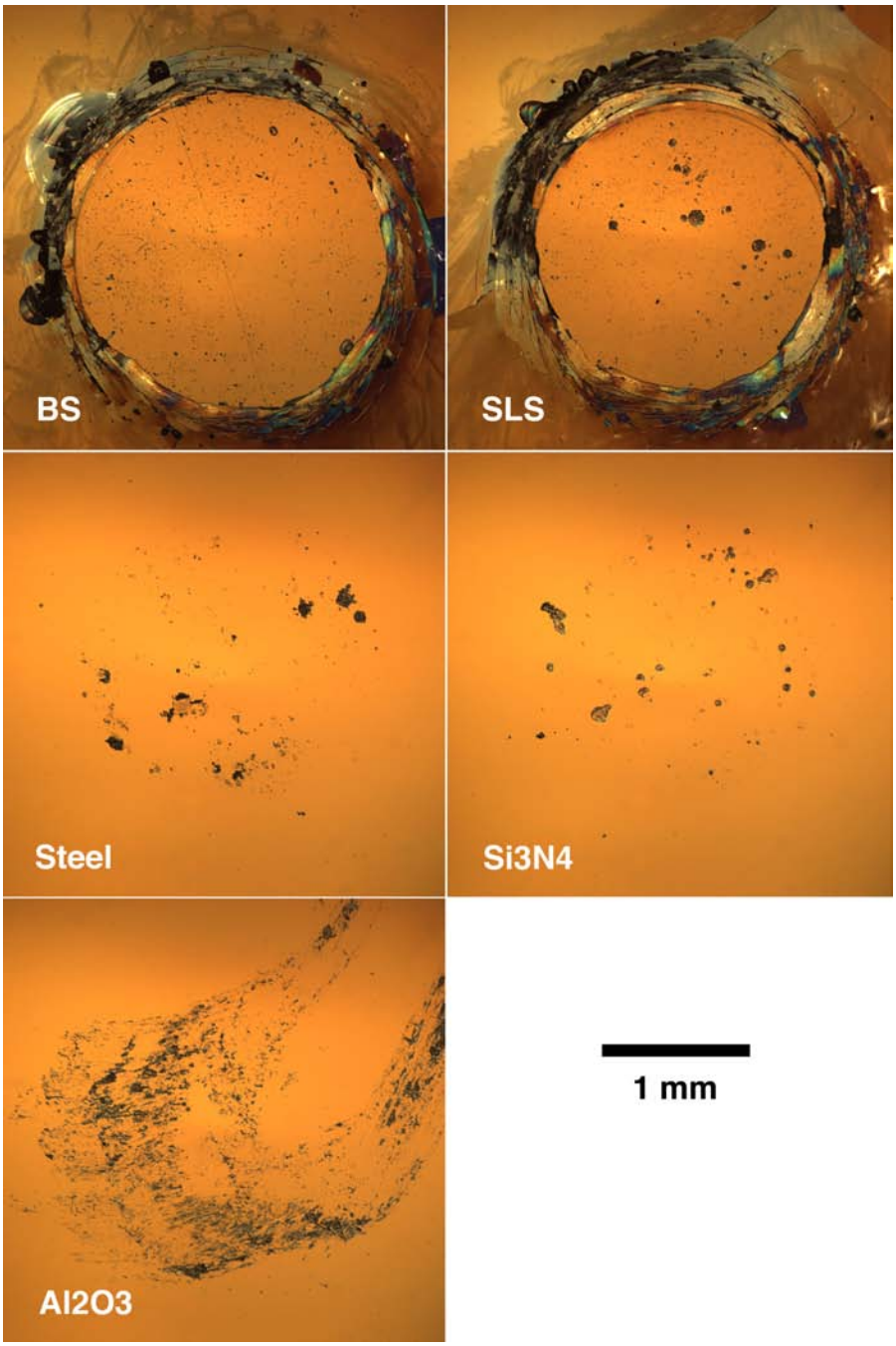

Figure 14. Comparison of contact locations for each of the five ball materials where the impact kinetic energies were equivalently valued (BS 576 mJ, SLS 623 mJ, steel 602 mJ, Si_3N_4 507 mJ, and Al_2O_3 590 mJ).

The trends of Fig. 14 show elastic property mismatches affect ring crack initiation at lower velocities and kinetic energies less than 1100 mJ. It is reasonable to believe its effect is contributing at higher velocities too; however, the density of the sphere (i.e., kinetic energy) more significantly affects the target response.

Lastly, the results from this work provide insights into what a suitable ball material could be to mimic rock strike testing of transparent armor. Among the five ball materials used in this study, silicon nitride is probably the closest match to "rock" in terms of both density and probably elastic modulus too. The BS and SLS ball materials have too low of a density and probably elastic moduli as well. Steel is too dense and plastically deforms that can produce a non-conservative fracture response in the Starphire SLS. Alumina is too stiff and has too high of a density. Mullite ($2SiO_2 \bullet 3Al_2O_3$ or $Al_6Si_2O_{13}$) has an attractive density (2.8 g/cm^3) and a low elastic modulus (150 GPa) but spheres of mullite were not commercially available at the beginning of this project; perhaps that has since changed.

6. SUMMARY

- Frictional effects contribute to fracture initiation in Starphire soda lime silicate (SLS) glass at low velocity impact.
- Spheres with a lower elastic modulus require less force to initiate fracture in Starphire SLS glass for both quasi-static spherical indentation testing and impact testing than spheres with a higher elastic modulus.
- Contact-induced fracture did not initiate in the Starphire SLS for impact kinetic energies up to ~ 150 mJ. For kinetic energies between ~ 150 - 1100 mJ, fracture sometimes initiated; however, it tended to occur when lower elastic modulus sphere were impacting it. Contact-induced fracture would always occur for impact energies > 1100 mJ.
- The force necessary to initiate contact-induced fracture is higher under dynamic conditions than it is under quasi-static conditions.
- Among the five used sphere materials, silicon nitride is the closest match to "rock" in terms of both density and probably elastic modulus. Mullite ($2SiO_2 \cdot 3Al_2O_3$) has an attractive density (2.8 g/cm^3) and a low elastic modulus (150 GPa) and may deserve more consideration as a future candidate sphere material (if a supplier can be found).

7. RECOMMENDATIONS FOR FUTURE WORK

- Measure elastic modulus and Poisson's ratio of typical rock materials.

- Pursue a fundamental understanding of why dynamic ring crack initiation occurs at higher forces than at slower, quasi-static conditions.

- Examine cone angle and its modeling with respect to the target's K_I/K_{II}.

- Conduct sphere impact testing as a function of temperature.

- Measure velocity of impact damage initiation when the target is under residual stress and contrast with responses of unstressed targets.

- Identify a source of mullite spheres for impact testing. Its material properties may be the most representative of "rock".

REFERENCES

[1] A. A. Wereszczak, W. L. Daloz, K. T. Strong, Jr., and O. M. Jadaan, "Effect of Indenter Elastic Modulus on Hertzian Ring Crack Initiation in Silicon Carbide," *Int. J. Appl. Cer. Tech.,* 8:885-94 (2011).

[2] A. D. Peralta and H. Yoshida, "Design of Impact-Resistant Ceramic Structural Components," Chapter 28 in *Ceramic Gas Turbine Component Development and Characterization, Volume 2*, Eds. M. van Roode, M. K. Ferber, and D. W. Richerson, ASME Press, New York, 2003.

[3] C. G. Knight, M. V. Swain, and M. M. Chaudhri, "Impact of Small Steel Spheres on Glass Surfaces", *J. Mat. Sci.*, 12:1573-86 (1977).

[4] S. Timoshenko and J. N. Goodier, *Theory of Elasticity*, McGraw-Hill Book Co., New York, 1951.

[5] K. L. Johnson, J. J O'Connor, and A. C. Woodward, "The Effect of the Indenter Elasticity on the Hertzian Fracture of Brittle Materials," *Proc. R. Soc. London,* 334:95-117 (1973).

[6] J. Dundurs, "Edge-Bounded Dissimilar Orthogonal Elastic Wedges Under Normal and Shear Loading," *J. Appl. Mech.*, 36:650-652 (1969).

[7] A. A. Wereszczak, T. P. Kirkland, K. T. Strong, Jr., and T. J. Holmquist, "ORNL Quasi-Static Mechanical Characterization and Analysis: FY09 Annual Report to TARDEC," ORNL/TM-2009/234 Report, December, 2009.

[8] A. A. Wereszczak, "Elastic Property Determination of WC Spheres and Estimation of Compressive Loads and Impact Velocities That Initiate Their Yielding and Cracking," *Cer. Eng. Sci. Proc.*, [7] 27:211-223 (2006).

[9] J. P. A. Tillett, "Fracture of Glass by Spherical Indenters," Proc. Phys. Soc. B., 69:47-54 (1956).

ACKNOWLEDGEMENTS

Research performed under Work For Others funded by U.S. Army Tank-Automotive Research, Development and Engineering Center, under contract DE-AC-00OR22725 with UT-Battelle, LLC.

The authors wish to express sincere appreciation to A. Dolan, F. Rickert, and D. Templeton of the U.S. Army Research, Development and Engineering Command - Tank-Automotive and Armaments Command for sponsoring this work. Additionally, Purdue University's W. Chen and M. Mordasky are thanked for their advice and guidance with the gas gun hardware design, ORNL's R. Wiles for his CAD assistance, and ORNL's M. Ferber for his assistance with the velocity measuring hardware and software. Lastly, the authors thank M. Ferber and R. Wiles for their review of this report and helpful comments.

This submission was produced by a contractor of the United States Government under contract DE-AC05-00OR22725 with the United States Department of Energy. The United States Government retains, and the publisher, by accepting this submission for publication, acknowledges that the United States Government retains, a nonexclusive, paid-up, irrevocable, worldwide license to publish or reproduce the published form of this submission, or allow others to do so, for United States Government purposes.

APPENDIX I

Sphere Material	Gas Gun Pressure (psi)	Velocity (m/s)	Kinetic Energy (mJ)	Visible Damage
Borosilicate	8	6.6	52	No
Borosilicate	8	10	119	No
Borosilicate	10	11.7	163	No
Borosilicate	10	12	171	No
Borosilicate	10	12	171	Sm Cone
Borosilicate	10	13.3	210	Scuff
Borosilicate	15	15.9	301	Scuff
Borosilicate	14	15.3	279	sm cone
Borosilicate	15	16.3	316	Med cone
Borosilicate	20	22	576	Med cone
Borosilicate	25	27.2	880	Med cone
SLS	8	10	135	No
SLS	10	11.3	172	No
SLS	10	12	194	Sm Cone
SLS	10	12	194	Sm Cone
SLS	12	14	264	No
SLS	13	15.3	316	scuff
SLS	12	15.4	320	Scuff
SLS	15	18.9	481	Med cone
SLS	20	21.4	617	Med cone
SLS	20	21.5	623	Med cone
SLS	20	22	652	
SLS	25	28.5	1095	Med cone
Si3N4	8	10	170	No
Si3N4	9	11	205	Scuff
Si3N4	10	12	244	Sm Cone
Si3N4	11	13	287	scuff
Si3N4	10	12.1	248	No
Si3N4	11	12.9	282	Sm Cone
Si3N4	11	13.5	309	Scuff

Si3N4	15	17.3	507	Scuff
Si3N4	20	23.6	944	No
Si3N4	25	27.6	1292	Sm Cone
Al2O3	8	9.8	201	Sm Cone
Al2O3	10	11.9	296	Scuff
Al2O3	10	12	301	Sm Cone
Al2O3	10	12.5	327	Scuff
Al2O3	12	13.9	404	Scuff
Al2O3	12	14.5	439	Sm ring
Al2O3	13	16.8	590	Scuff
Al2O3	15	17	604	Sm Cone
Al2O3	15	17	604	Sm ring
Al2O3	20	20.8	904	Sm ring
Al2O3	25	30.5	1944	Full cone
Steel	8	10.2	435	No
Steel	10	11.5	553	Scuff
Steel	10	12	602	Scuff
Steel	12	14	819	Scuff
Steel	13	16.1	1083	Scuff
Steel	15	17	1208	sm-med cone
Steel	15	18.2	1385	Med cone
Steel	15	18.9	1493	Sm cone
Steel	15	19.1	1525	Med cone
Steel	20	23.5	2308	Lg cone
Steel	25	27.9	3254	Full cone

* Red velocity value indicates an estimated velocity from gas pressure, not measured by the sensor system. Grayed line is the identified speed where ring crack initiation initiated.